Inclusive B-meson production at the LHC in the general-mass variable-flavor-number scheme

B. A. Kniehl,[1] G. Kramer,[1] I. Schienbein,[2] and H. Spiesberger[3]

[1]*II. Institut für Theoretische Physik, Universität Hamburg, Luruper Chaussee 149, D-22761 Hamburg, Germany*
[2]*Laboratoire de Physique Subatomique et de Cosmologie, Universite Joseph Fourier Grenoble 1, CNRS/IN2P3, Institut National Polytechnique de Grenoble, 53 avenue des Martyrs, F-38026 Grenoble, France*
[3]*Institut für Physik, Johannes-Gutenberg-Universität, Staudinger Weg 7, D-55099 Mainz, Germany*
(Received 12 September 2011; published 21 November 2011)

We calculate the next-to-leading-order cross section for the inclusive production of B mesons in pp collisions in the general-mass variable-flavor-number scheme, an approach that takes into account the finite mass of the b quarks. We use realistic evolved nonperturbative fragmentation functions obtained from fits to e^+e^- data and compare our results for the transverse-momentum and rapidity distributions at a center-of-mass energy of 7 TeV with recent data from the CMS Collaboration at the CERN LHC. We find good agreement, in particular, at large values of p_T.

DOI: 10.1103/PhysRevD.84.094026 PACS numbers: 12.38.Bx, 12.39.St, 13.85.Ni, 14.40.Nd

I. INTRODUCTION

Since the late eighties there has been much interest in the study of B-meson production in $p\bar{p}$ and pp collisions at hadron colliders, both experimentally and theoretically. The first measurements were performed more than two decades ago by the UA1 Collaboration at the CERN $Sp\bar{p}S$ collider [1] operating at a center-of-mass energy of $\sqrt{S} = 0.63$ TeV. More recent measurements were made by the CDF and D0 collaborations at the Fermilab Tevatron running at $\sqrt{S} = 1.8$ TeV [2,3] and 1.96 TeV [4]. Just recently, the CMS Collaboration at the CERN LHC collider published first results for inclusive B^+- [5], B^0- [6], and B_s-meson [7] production in pp collisions at $\sqrt{S} = 7$ TeV. B^+ mesons were reconstructed via their decay $B^+ \to J/\psi K^+$ followed by $J/\psi \to \mu^+\mu^-$, whereas B^0 mesons were identified through the observation of $J/\psi K_s^0$ final states with the subsequent decays $J/\psi \to \mu^+\mu^-$ and $K_s^0 \to \pi^+\pi^-$. In the case of B_s mesons, the reconstructed final states were generated by the decay chain $B_s \to J/\psi\phi$, $J/\psi \to \mu^+\mu^-$, and $\phi \to K^+K^-$. From all these measurements the differential cross sections $d\sigma/dp_T$ and $d\sigma/dy$ as well as the integrated cross section for $p_T \geq 5$ GeV (for B^+ and B^0 mesons) or $p_T \geq 8$ GeV (for B_s mesons) were reported.

The general-mass variable-flavor-number (GM-VFN) scheme provides a rigorous theoretical framework for the description of the inclusive production of single heavy-flavored hadrons, combining the fixed-flavor-number (FFN) [8] and zero-mass variable-flavor-number (ZM-VFN) [9] schemes, which are valid in complementary kinematic regions, in a unified approach that enjoys the virtues of both schemes and, at the same time, is bare of their flaws. Specifically, it resums large logarithms by the Dokshitzer-Gribov-Lipatov-Altarelli-Parisi (DGLAP) evolution of nonperturbative fragmentation functions (FFs), guarantees the universality of the latter as in the ZM-VFN scheme, and simultaneously retains the mass-dependent terms of the FFN scheme without additional theoretical assumptions. It was elaborated at next-to-leading order (NLO) for photoproduction [10] and hadroproduction [11] of charmed hadrons as well as for their production by e^+e^- annihilation [12]. It was also applied to obtain predictions for B-meson hadroproduction [13], which could be compared with recent CDF data [4]. An earlier implementation of such an interpolating scheme is the so-called fixed-order-next-to-leading-logarithm approach, in which the conventional cross section in the FFN scheme is linearly combined, with the help of a p_T-dependent weight function, with a suitably modified cross section in the ZM-VFN scheme implemented with perturbative FFs [14].

In Ref. [13], nonperturbative FFs for the transitions $a \to B$, where a is any parton, including b and $\bar{b}$ quarks, were extracted at NLO in the $\overline{\text{MS}}$ factorization scheme with $n_f = 5$ flavors from the scaled-energy (x) distributions $d\sigma/dx$ of $e^+e^- \to B + X$ measured by the ALEPH [15] and OPAL [16] collaborations at the CERN LEP1 collider and by the SLD Collaboration [17] at the SLAC SLC collider. As explained in Ref. [13], these FFs may be consistently used in our GM-VFN framework. Working at NLO in the GM-VFN scheme with these B-meson FFs, we found excellent agreement with recent CDF measurements of $d\sigma/dp_T$ for $p\bar{p} \to B + X$ [4], especially in the upper p_T range, $p_T \gtrsim 10$ GeV [13].

The content of this paper is as follows. In Sec. II, we summarize our input choices of parton distribution functions (PDFs) and B-meson FFs. In Sec. III, we compare the predictions of the GM-VFN scheme with the CMS data from the recent LHC run at $\sqrt{S} = 7$ TeV [5–7]. Our conclusions are given in Sec. IV.

II. INPUT PDFS AND B-MESON FFS

As PDFs for the proton, we choose one of the most recent parametrizations of the CTEQ Collaboration, set CTEQ6.6M [18], which provides an improvement over

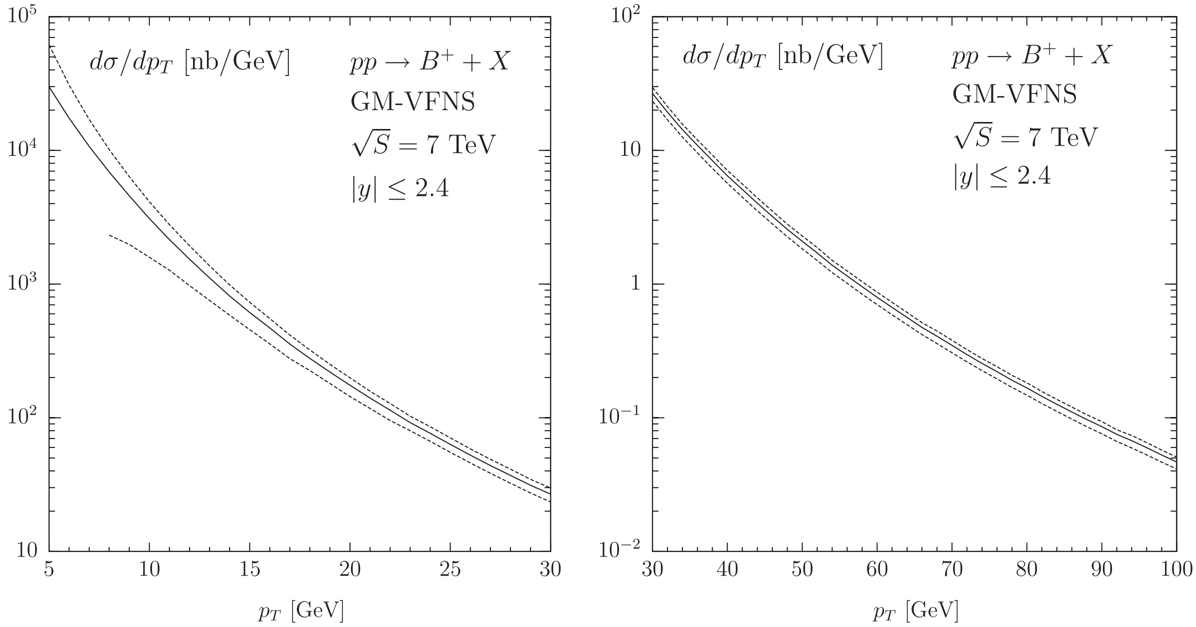

FIG. 1. $d\sigma/dp_T$ [nb/GeV] for $pp \to B^+ + X$ at $\sqrt{S} = 7$ TeV in the GM-VFN scheme. For clarity, we split the p_T range into a lower part (p_T below 30 GeV, left) and an upper part (p_T above 30 GeV, right). The central values (solid lines) correspond to the default choice of scale parameters, $\xi_R = \xi_F = 1$. An error band (dashed lines) is obtained from variations of the renormalization and factorization scales by factors of 2 up and down. The upper end of the error band is reached for $\xi_R = 1$ and $\xi_F = 2$ at $p_T < 21$ GeV and for $\xi_R = 0.5$ and $\xi_F = 1$ at $p_T > 21$ GeV, the lower error end is reached for $\xi_R = 1$ and $\xi_F = 0.5$ at $p_T < 25$ GeV and $\xi_R = 2$ and $\xi_F = 1$ at $p_T > 25$ GeV.

the earlier version CTEQ6.5M. Both sets were obtained in the framework of a general-mass scheme using the input values $m_c = 1.3$ GeV, $m_b = 4.5$ GeV, and $\alpha_s(m_Z) = 0.118$. In both sets, the b-quark PDF has its starting scale at $\mu_0 = m_b$.

The nonperturbative FFs describing the transition of the b and $\bar{b}$ quarks into a B meson can be obtained only from experiment. In our earlier work on inclusive B-meson production at the Tevatron [13], we constructed such FFs using as input recent precise measurements of the cross section of inclusive B-meson production in e^+e^- annihilation obtained by the ALEPH [15], OPAL [16], and SLD [17] collaborations.[1] These data were taken on the Z-boson resonance, so that finite-m_b effects, being of relative order m_b^2/m_Z^2, are strongly suppressed, which means that we are in the asymptotic regime where the GM-VFN scheme is equivalent to the ZM-VFN scheme. The combined fit to the three data sets was performed using the NLO value $\Lambda^{(5)}_{\overline{MS}} = 227$ MeV corresponding to $\alpha_s^{(5)}(m_Z) = 0.1181$, values adopted from Ref. [18]. The renormalization and factorization scales were chosen to be $\mu_R = \mu_F = m_Z$. In accordance with the chosen PDFs, the starting scale of the $b \to B$ FF was taken to be $\mu_0 = m_b$, while the $g, q \to B$ FFs, where q denotes the light quarks including the charm quark, were taken to vanish at $\mu_F = \mu_0$.

For fitting the data, we actually employed two different parametrizations for the $b \to B$ FF at $\mu_0 = m_b$, namely, the Peterson ansatz [20] and the simple power ansatz [21]. It turned out that the Peterson ansatz led to a very poor fit. Therefore, we shall use in this work only the FFs obtained with the power ansatz, whose parameters at the starting scale are listed in Table 1 of Ref. [13]. A comparison of the fit performed using this ansatz with the three input data sets may be found in Fig. 1 of that reference.

We note that the data from OPAL and SLD included all B-hadron final states, in particular, those with Λ_b hadrons, while, in the ALEPH analysis, only final states with identified $B^\pm$ and B^0 mesons were taken into account. Our fit was based on the assumption that the FFs of all b hadrons had the same shape. The branching fraction of $b \to B^+$ was taken equal to that of $b \to B^0$ and fixed to 0.397. In our calculations for B_s-meson production to be presented below, we shall use the same FFs and rescale them by the factor 0.113/0.401, which uses the up-to-date values for the $b \to B^+$ and $b \to B_s$ branching fractions quoted by the Particle Data Group [22].

We should emphasize that, in the analysis of the available e^+e^- annihilation data, the charged and neutral B mesons were not separated. Furthermore, the charged states B^+ and B^- could not be distinguished. The FFs obtained in Ref. [13] are, therefore, valid for the average of B^+ and B^- and, similarly, for the average of B^0 and $\bar{B}^0$.

The factorization scales related to the initial- and final-state singularities entering the PDFs and FFs, respectively,

[1]Recently, similar data have become available also from the DELPHI Collaboration [19].

can in principle be chosen independently. We checked, however, that when estimating theoretical error bands by varying these scales by factors of 2 up and down, the extreme values are indeed obtained when the initial- and final-state factorization scales are identified. Our default choice of renormalization and factorization scales is $\mu_R = \mu_F = m_T = \sqrt{p_T^2 + m_b^2}$. Theoretical uncertainties will be estimated by setting $\mu_R = \xi_R m_T$ and $\mu_F = \xi_F m_T$, and varying ξ_R and ξ_F about their default values $\xi_R = \xi_F = 1$ by factors of 2 up and down, restricting the ratio to the range $1/2 \leq \xi_R/\xi_F \leq 2$.

III. THEORETICAL PREDICTIONS FOR $pp \to B + X$ AND COMPARISONS WITH CMS DATA

To obtain an overview of the p_T dependence of $d\sigma/dp_T$, we first show results for this observable, integrated over $|y| \leq 2.4$, for the case of B^+ production in the GM-VFN scheme as described above. This differential cross section is shown in Fig. 1 (left) for p_T values between 5 and 30 GeV and in Fig. 1 (right) for larger p_T values, up to 100 GeV, where we expect data to come in the near future when the LHC experiments will have accumulated more statistics.

In the p_T range between 5 and 30 GeV, the cross section falls off by 3 orders of magnitude. This is essentially due to the behavior of the PDFs as a function of the scaling variable x and less so due to the behavior of the partonic cross sections. Towards low p_T values, both the upper edge of the error band and the cross section for the default choice of scales rise steadily with decreasing p_T value, down to $p_T = 5$ GeV. This is caused by the scale dependence of the b-quark PDF and the FFs. With our choice of scales, they fade out and quench the cross section, leading to a turnover of the p_T distributions only at $p_T = 0$ and not already at some finite p_T value. The lower edge of the error band is obtained for $\xi_F = 0.5$. Here, both the b-quark PDF and the FFs vanish at $p_T \approx 8$ GeV, corresponding to $\mu_F = m_b = 4.5$ GeV. The line representing the lower edge of the error band therefore stops at this point.

The CMS Collaboration measured the differential cross section $d\sigma/dp_T$ for the production of B^+ mesons [5] (actually the average of B^+ and B^- mesons), integrated over the y range $|y| \leq 2.4$, as a function of p_T. The measurement covered the p_T range from 5 GeV to 30 GeV with five bins. In addition, the differential cross section $d\sigma/d|y|$, integrated over the considered p_T range, was given for six $|y|$ bins. In Ref. [6], the results of the measurement of B^0-meson production (again for the average of the charge-conjugate states B^0 and $\bar{B}^0$) were presented. They comprise the differential cross section $d\sigma/dp_T$, integrated over the y range $|y| \leq 2.2$, in five p_T bins between $p_T = 5$ GeV and $p_T = 40$ GeV and $d\sigma/d|y|$, integrated over the considered p_T range, in five $|y|$ bins. Since, in this second analysis, a larger luminosity was already available, the B^0 data extend to larger p_T values.

In order to facilitate the comparisons with the CMS measurements [5,6], we integrate over the bins using the same binnings. The p_T bins for B^+- and B^0-meson production are the same, except for the largest one. Our results are shown in Figs. 2 and 3, where they are compared with the experimental data. The errors of the experimental data points are obtained from Ref. [6] by adding in quadrature the statistic and systematic errors quoted there. The differences between the predictions in Figs. 2 and 3 are entirely due to the different bin choices, the FFs being the same in both cases.

We determine the error band from variations of the scale parameters by factors of 2 as described above, except that the minimum of the theoretical prediction is obtained with the additional prescription that the FFs are frozen when μ_F falls below the starting scale $\mu_0 = m_b$. Otherwise the cross section would become zero for $\xi_F = 0.5$ in a large part of the first p_T bin, so that the lower edge of the error band would become meaningless. As is seen in Figs. 2 and 3, the data lie inside the error bands. In the case of B^+ (B^0) mesons, the default predictions appreciably overshoot the CMS data in the first three (two) p_T bins, while they are very close to the CMS data in the residual p_T bins. The default values of the predicted cross sections are a factor of approximately 2 (1.5) larger than the experimental central values in the lowest (next-to-lowest) p_T bins. This is caused by the fact that, with our choice of scales, large contributions coming from initial-state b quarks are present for all finite values of p_T. If one changes the factorization scale to a lower value, for example, by setting $\xi_R = 1$ and $\xi_F = 0.7$, the b-quark PDF vanishes at $p_T = 4.6$ GeV. Furthermore, with our prescription, the PDFs and the FFs are frozen at the values they reach at $\mu_F = m_b$ when p_T falls below $p_T = 4.6$ GeV. For this special choice of factorization scales, we obtain the cross section values given for the B^0-meson case in the column labeled $\xi_R = 1$, $\xi_F = 0.7$ of Table I. For comparison, we present the experimental results in the second column of this table and the default-scale results of Fig. 3 (left) in the third one. We see that the theoretical values of the cross sections in the five p_T bins agree with the experimental values quite well, within the errors. The total B^0-meson production cross section determined by CMS in the considered kinematic range is $\sigma_{\rm tot} = 33.2 \pm 4.3$ μb. For the default choice of scales $\xi_R = \xi_F = 1$, we find $\sigma_{\rm tot} = 61.7$ μb, while the result for $\xi_R = 1$ and $\xi_F = 0.7$ is 35.0 μb, in very good agreement with the data. A similar comparison may be performed for $pp \to B^+X$, with similar conclusions, as can be inferred from Fig. 2 (right panel), where we show the corresponding results for $d\sigma/d|y|$. The theoretical predictions are almost identical, since the FFs for $b \to B^+$ and $b \to B^0$ are taken to be the same and there

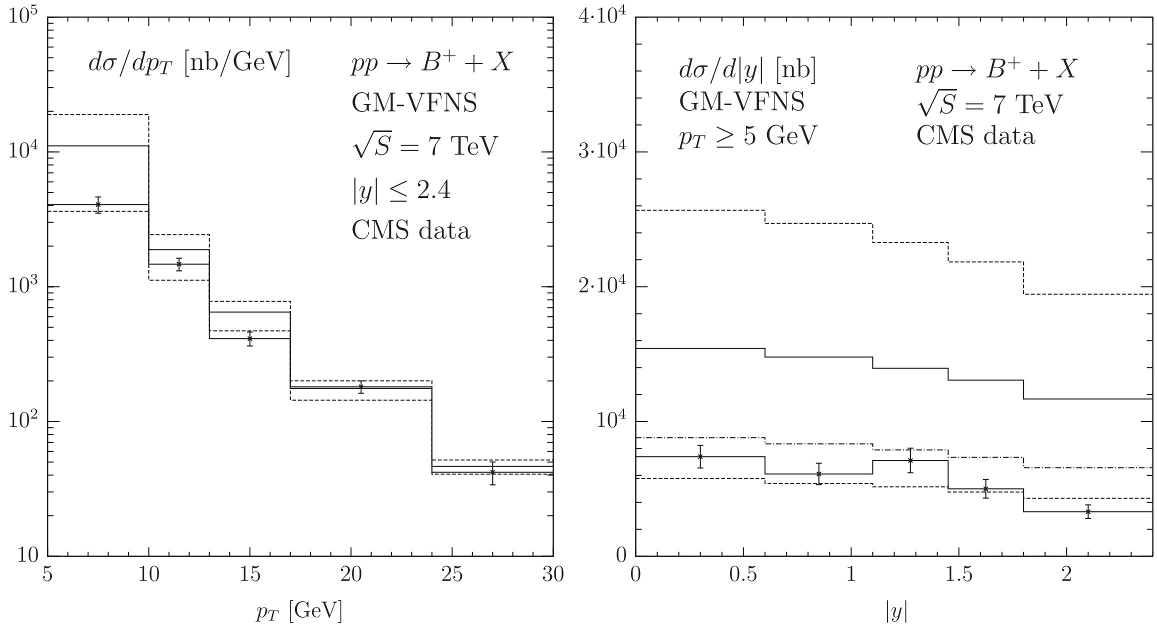

FIG. 2. $d\sigma/dp_T$ [nb/GeV] (left) and $d\sigma/d|y|$ [nb] (right) for $pp \to B^+ + X$ at NLO in the GM-VFN scheme compared with the CMS data [5]. The central values (solid lines) correspond to the choice $\xi_R = \xi_F = 1$. We also show the prediction for $d\sigma/d|y|$ obtained with the choice $\xi_R = 1$ and $\xi_F = 0.7$ (dashed-dotted line). The error bands (dashed lines) are obtained by varying ξ_R and ξ_F by factors of 2 up and down (maximum: $\xi_R = 1$, $\xi_F = 2$; minimum: $\xi_R = 1$, $\xi_F = 0.5$).

is only a tiny difference due to the different upper ends of the p_T ranges.

As explained above, massless contributions, in particular, the ones due to incoming b quarks, dominate the total cross section towards low p_T values. These contributions lead to an increase of $d\sigma/dp_T$ in the limit $p_T \to 0$ because the heavy-quark PDFs carry resummed logarithms, which are not fully cancelled by the subtraction terms in the GM-VFN approach, which are implemented at NLO, i.e. at fixed order only. This increase can be tamed by imposing

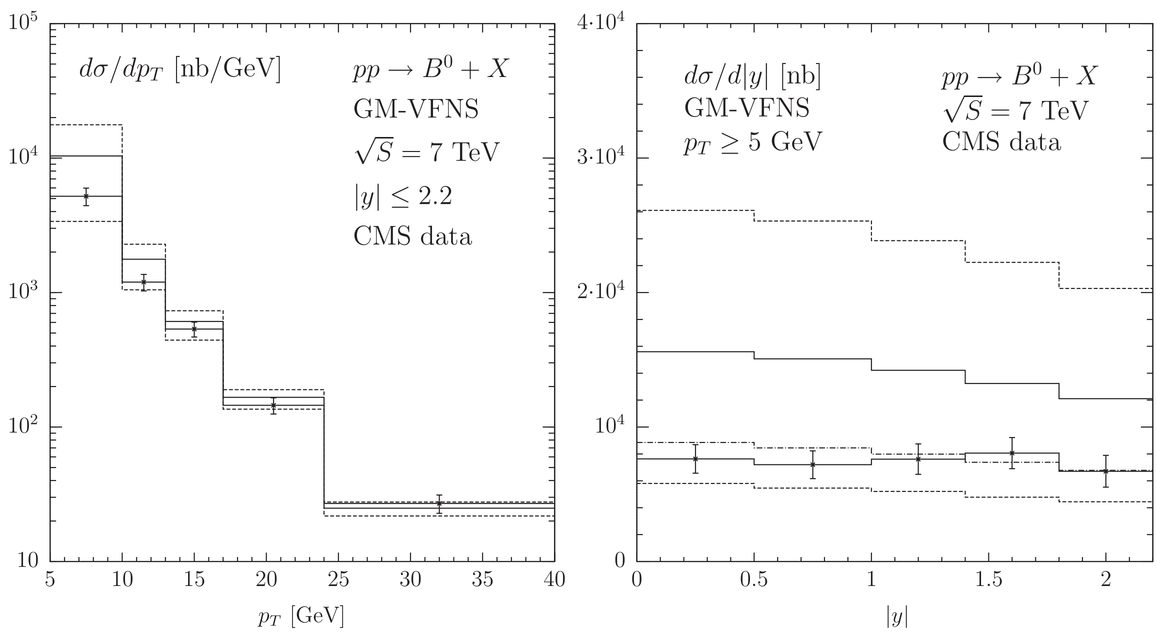

FIG. 3. $d\sigma/dp_T$ [nb/GeV] (left) and $d\sigma/d|y|$ [nb] (right) for $pp \to B^0 + X$ at NLO in the GM-VFN scheme compared with the CMS data [6]. The central values (solid lines) correspond to the choice $\xi_R = \xi_F = 1$. We also show the prediction for $d\sigma/d|y|$ obtained with the choice $\xi_R = 1$ and $\xi_F = 0.7$ (dashed-dotted line). The error bands (dashed lines) are obtained by varying ξ_R and ξ_F by factors of 2 up and down (maximum: $\xi_R = 1$, $\xi_F = 2$; minimum: $\xi_R = 1$, $\xi_F = 0.5$).

TABLE I. Predictions for the differential cross section $d\sigma/dp_T$ [nb/GeV] of B^0-meson production with different renormalization and factorization scales compared with the CMS data [6], for which the statistical and systematic errors are added in quadrature. The values presented in the second and third columns are also displayed in Fig. 3 (left).

p_T (in GeV)	Data [6]	$\xi_R = \xi_F = 1$	$\xi_R = 1$, $\xi_F = 0.7$	$\xi_a = 0.2$
5–10	5200 ± 770	10 356	5578	6327
10–13	1196 ± 168	1769	1265	1016
13–17	535 ± 68	610	481	401
17–24	145 ± 20	166	141	124
24–40	27 ± 4	25	22	21

the kinematic cut $\hat{s} > 4m_b^2$ on the square of the partonic center-of-mass energy $\hat{s}$ also for the massless contributions. Furthermore, a judicious choice of the factorization scale, e.g.

$$\mu_F = \sqrt{m_b^2 + \xi_a p_T^2}, \tag{1}$$

with a parameter $\xi_a < 1$, can boost the transition $\mu_F \to \mu_0 = m_b$ for $p_T \to 0$. This prescription creates a turnover of the p_T distribution towards low p_T values and also allows us to obtain a reasonable description of the CDF data [4], which were taken at lower p_T values. The CMS data start at $p_T = 5$ GeV, and a turnover is not visible in $d\sigma/dp_T$. However, the ansatz of Eq. (1) leads to a reduction of the p_T distribution for small p_T values, i.e. to a significant change of $d\sigma/dp_T$ in the first two p_T bins. The cross section values obtained for B^0 mesons using the scale choice of Eq. (1) with $\xi_a = 0.2$ are presented in the last column of Table I. We find that this approach leads to a better description of the CMS data, which is, however, not as good as for the scale choice $\xi_F = 0.7$ (fourth column of Table I).

As a side remark, we note that the behavior towards small p_T values is not due to a shift in the average B-meson to b-quark momentum fraction. This may be observed by calculating the quantity

$$\langle z\rangle(p_T) = \frac{\int dz z d\sigma(p_T)}{\int dz d\sigma(p_T)},$$

where z is the scaling variable of the FFs and it is understood that the integration is also done over the rapidity interval $|y| \leq 2.4$ relevant for the CMS measurement [5]. We find a rather weak dependence on p_T. In fact, $\langle z\rangle$ decreases from 0.770 at $p_T = 5$ GeV to 0.749 at $p_T = 30$ GeV, which means that, in our applications, the $b \to B$ FF is always probed around its maximum (see Ref. [13]).

We now discuss the $|y|$ distributions $d\sigma/d|y|$ of B^+ and B^0 production shown in the right panels of Figs. 2 and 3, respectively. The bulk of these cross sections comes from the lowest p_T bin, where the theoretical uncertainties are largest, as is evident from Table I. However, it is interesting to find out how much the shapes of these differential cross

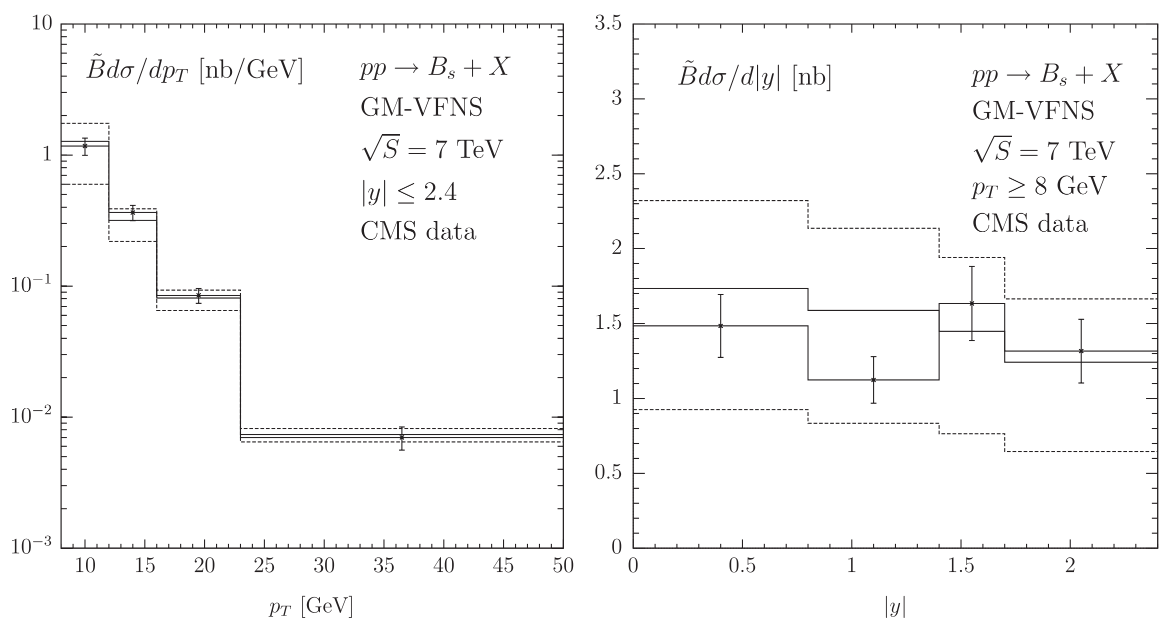

FIG. 4. $\tilde{B}d\sigma/dp_T$ [nb/GeV] (left) and $\tilde{B}d\sigma/d|y|$ [nb] (right) for $pp \to B_s + X$ at NLO in the GM-VFN scheme compared with the CMS data [7]. The branching fraction of the decay $B_s \to J/\psi\phi$ is assumed to be $\tilde{B} = 1.3 \times 10^{-3}$ [22]. The central values (solid lines) correspond to the choice $\xi_R = \xi_F = 1$. The error bands (dashed lines) are obtained by varying ξ_R and ξ_F by factors of 2 up and down (maximum: $\xi_R = 0.5$, $\xi_F = 1$; minimum: $\xi_R = 1$, $\xi_F = 0.5$).

sections depend on the various scale choices. In order to get some idea about this, we include in the right panels of Figs. 2 and 3 as dotted-dashed histograms also the predictions evaluated using the scale choice $\xi_R = 1$ and $\xi_F = 0.7$, as in the fourth column in Table I. They agree fairly well with the CMS data, while the default predictions ($\xi_R = \xi_F = 1$), shown as solid histograms, significantly overshoot the CMS data as expected, but their shapes are still reasonable.

Finally, in Fig. 4, we present our predictions for the production of B_s mesons and compare them with the experimental data published by the CMS Collaboration in Ref. [7]. $d\sigma/dp_T$ was measured in four p_T bins between $p_T = 8$ and 50 GeV and integrated over $|y| \leq 2.4$, and $d\sigma/d|y|$ was measured in four $|y|$ bins spanning this $|y|$ range and integrated over the full p_T range considered. Both the experimental data and our theoretical predictions refer to the product of cross section times branching fraction $\tilde{B}$ for $B_s \to J/\psi\phi$, for which we adopt the value 1.3×10^{-3} from Ref. [22]. In this case, we find better agreement between theory and experiment over the full p_T range, probably due to the fact that very low values of p_T, with $p_T < 8$ GeV, are excluded from this analysis. The total cross section times branching fraction measured by CMS for 8 GeV $\leq p_T \leq$ 50 GeV and $|y| \leq 2.4$ is 6.9 ± 0.8 nb, while our calculation yields 7.2 nb.

IV. CONCLUSIONS

In summary, we applied the GM-VFN scheme to obtain NLO predictions for the production of B mesons in pp collisions at the LHC. The comparison with experimental data from the CMS Collaboration at $\sqrt{S} = 7$ TeV generally shows good agreement between theory and experiment, in particular, at large p_T values. The agreement is particularly good for the case of B_s-meson production, where data are restricted to p_T values above 8 GeV. At low p_T values, we observe large scale uncertainties.

Future data collection at the LHC will allow us to extend the comparisons with theoretical predictions to much wider p_T ranges. If also the systematic uncertainties can be further reduced, we may expect that B-meson production will play an increasingly important role in constraining size and shape of both PDFs and FFs.

ACKNOWLEDGMENTS

This work was supported in part by the German Federal Ministry for Education and Research BMBF through Grant No. 05 HT6GUA, by the German Research Foundation DFG through the Collaborative Research Centre No. 676 *Particles, Strings and the Early Universe—The Structure of Matter and Space Time*, and by the Helmholtz Association HGF through the Helmholtz Alliance Ha 101 *Physics at the Terascale*.

[1] C. Albajar *et al.* (UA1 Collaboration), Phys. Lett. B **213**, 405 (1988).

[2] F. Abe *et al.* (CDF Collaboration), Phys. Rev. Lett. **75**, 1451 (1995); D. E. Acosta *et al.* (CDF Collaboration), Phys. Rev. D **66**, 052005 (2002).

[3] S. Abachi *et al.* (D0 Collaboration), Phys. Rev. Lett. **74**, 3548 (1995); B. Abbott *et al.* (D0 Collaboration), Phys. Rev. Lett. **84**, 5478 (2000).

[4] D. Acosta *et al.* (CDF Collaboration), Phys. Rev. D **71**, 032001 (2005); A. Abulencia *et al.* (CDF Collaboration), Phys. Rev. D **75**, 012010 (2007); T. Aaltonen *et al.* (CDF Collaboration), Phys. Rev. D **79**, 092003 (2009).

[5] V. Khachatryan *et al.* (CMS Collaboration), Phys. Rev. Lett. **106**, 112001 (2011).

[6] S. Chatrchyan *et al.* (CMS Collaboration), Phys. Rev. Lett. **106**, 252001 (2011).

[7] S. Chatrchyan *et al.* (CMS Collaboration), Phys. Rev. D **84**, 052008 (2011).

[8] P. Nason, S. Dawson, and R. K. Ellis, Nucl. Phys. **B303**, 607 (1988); **B327**, 49 (1989); **B335**, 260(E) (1989); W. Beenakker, H. Kuijf, W. L. van Neerven, and J. Smith, Phys. Rev. D **40**, 54 (1989); W. Beenakker, W. L. van Neerven, R. Meng, G. A. Schuler, and J. Smith, Nucl. Phys. **B351**, 507 (1991); I. Bojak and M. Stratmann, Phys. Rev. D **67**, 034010 (2003).

[9] M. Cacciari and M. Greco, Nucl. Phys. **B421**, 530 (1994); B. A. Kniehl, M. Krämer, G. Kramer, and M. Spira, Phys. Lett. B **356**, 539 (1995); M. Cacciari, M. Greco, B. A. Kniehl, M. Krämer, G. Kramer, and M. Spira, Nucl. Phys. **B466**, 173 (1996); J. Binnewies, B. A. Kniehl, and G. Kramer, Z. Phys. C **76**, 677 (1997); B. A. Kniehl, G. Kramer, and M. Spira, Z. Phys. C **76**, 689 (1997); J. Binnewies, B. A. Kniehl, and G. Kramer, Phys. Rev. D **58**, 014014 (1998); **58**, 034016 (1998); B. A. Kniehl and G. Kramer, Phys. Rev. D **60**, 014006 (1999); B. A. Kniehl, in *Proceedings of the 14th Topical Conference on Hadron Collider Physics: Hadron Collider Physics 2002, Karlsruhe, Germany*, edited by M. Erdmann and Th. Müller (Springer, Berlin, 2003), p. 161; B. A. Kniehl and G. Kramer, Phys. Rev. D **71**, 094013 (2005); **74**, 037502 (2006).

[10] G. Kramer and H. Spiesberger, Eur. Phys. J. C **22**, 289 (2001); **28**, 495 (2003); **38**, 309 (2004); B. A. Kniehl, G. Kramer, I. Schienbein, and H. Spiesberger, Eur. Phys. J. C **62**, 365 (2009); G. Kramer and H. Spiesberger, Phys. Lett. B **679**, 223 (2009).

[11] B. A. Kniehl, G. Kramer, I. Schienbein, and H. Spiesberger, Phys. Rev. D **71**, 014018 (2005); Eur. Phys.

J. C **41**, 199 (2005); AIP Conf. Proc. **792**, 867 (2005); Phys. Rev. Lett. **96**, 012001 (2006); Phys. Rev. D **79**, 094009 (2009).

[12] T. Kneesch, B. A. Kniehl, G. Kramer, and I. Schienbein, Nucl. Phys. **B799**, 34 (2008).

[13] B. A. Kniehl, G. Kramer, I. Schienbein, and H. Spiesberger, Phys. Rev. D **77**, 014011 (2008).

[14] M. Cacciari, M. Greco, and P. Nason, J. High Energy Phys. 05 (1998) 007; M. Cacciari and P. Nason, Phys. Rev. Lett. **89**, 122003 (2002); M. Cacciari, P. Nason, and C. Oleari, J. High Energy Phys. 04 (2006) 006.

[15] A. Heister *et al.* (ALEPH Collaboration), Phys. Lett. B **512**, 30 (2001).

[16] G. Abbiendi *et al.* (OPAL Collaboration), Eur. Phys. J. C **29**, 463 (2003).

[17] K. Abe *et al.* (SLD Collaboration), Phys. Rev. D **65**, 092006 (2002); **66**, 079905(E) (2002).

[18] P. M. Nadolsky *et al.* (CTEQ Collaboration), Phys. Rev. D **78**, 013004 (2008).

[19] J. Abdallah *et al.* (DELPHI Collaboration), Eur. Phys. J. C **71**, 1557 (2011).

[20] C. Peterson, D. Schlatter, I. Schmitt, and P. M. Zerwas, Phys. Rev. D **27**, 105 (1983).

[21] V. G. Kartvelishvili and A. K. Likhoded, Yad. Fiz. **42**, 1306 (1985) [Sov. J. Nucl. Phys. **42**, 823 (1985)].

[22] K. Nakamura *et al.* (Particle Data Group), J. Phys. G **37**, 075021 (2010).